International Journal of Materials Engineering and Technology

Published Online: January 2015
Available online at http://www.pphmj.com/journals/ijmet.htm
Volume 13, Number 1, 2015, Pages 81-108 **ISSN: 0975-0444**

ANALYSIS OF BUCKLING BEHAVIOR OF ELLIPTICAL PLATE WITH NON-CONCENTRIC ELLIPTIC HOLE

Salahaddin Sanusei[1], Emad Mazhari[1] and Alireza Shahidi[2]

[1]Oakland University
2200 N. Squirrel Road Rochester
Michigan 48309-4401, U. S. A.

[2]Isfahan University of Technology
Isfahan, Iran

Abstract

This study is conducted to analyze the buckling behavior of elliptical homogeneous plates with a non-concentric elliptic hole subjected to uniform radial loading under different boundary conditions using Rayleigh-Ritz method. The geometry of plate with a non-concentric elliptic hole through a proper mapping transfers to natural coordinate system. Consequently, in-plane and out-of-plane displacement fields with respect to natural coordinates system are expressed using the Hierarchical, Hermitian, Lagrange and Fourier series shape functions. The Kirchhoff theory is used to formulate the problem in buckling condition. Due to the asymmetry in geometry, the in-plane solution is required to find the stress distribution. In terms of effects of the elliptic hole eccentricity, results show that the hole eccentricity has an insignificant effect on the critical buckling load factor in simply supported boundary conditions cases.

Received: September 8, 2014; Accepted: October 8, 2014

Keywords and phrases: buckling, elliptical plate, non-concentric hole, shape function, Rayleigh-Ritz method.

Nomenclature

$\mathbf{K}_b$	bending stiffness matrix
$\mathbf{K}_G$	geometric stiffness matrix
x, y	Cartesian coordinates
N_{cr}	critical load
ξ, η	natural coordinates
λ	buckling load factor
λ_{cr}	critical buckling load factor
$\mathbf{K}_{ml}$	plate's membrane stiffness matrix
N_{ui}, N_{vi}, N_{wi}	vectors of interpolation functions
$\boldsymbol{\Delta}$	generalized coordinates
D	flexural rigidity
$\boldsymbol{\kappa}$	curvature vector
U_b	strain energy due to the bending moment
W	work done on the mid-plane of plate due to the external forces
$\boldsymbol{\sigma}$	in-plane stress matrix
Π	total potential energy
U_{ml}	strain energy due to in-plane deformation
$\boldsymbol{\varepsilon}_{ml}$	in-plane strains vector
W_t	work done by the applied traction load
$\mathbf{t}$	traction vector
$\mathbf{F}$	generalized force vector

1. Introduction

By definition, buckling is a mechanical instability of a structure that is resulted from critical load. This critical load causes a column to fail. In contrast, due to membranes behavior, a plate can sustain more than its critical

buckling load. This phenomenon is called *post buckling behavior* of plate, therefore, critical buckling load is the starting point for post buckling behavior.

Timoshenko and Woinowsky [1] and Ugural [2] have set the milestone work on plates and shells. Since then, numerous researches and studies have been done to calculate the force or displacement which causes buckling in a plate by considering different geometry. Using Rayleigh-Ritz method, Jazi and Farhatnia [3] investigated the buckling analysis of functionally graded super-elliptical plate with clamped and simply supported boundary conditions under uniform radial loading. Using the finite difference method, Reddy and Alwar [4] studied the post buckling behavior of isotropic and orthotropic annular plates under uniform radial loading inside the hole and on the outer border, with different boundary conditions. The Rayleigh-Ritz method is used by Altekin [5] to investigate the free linear vibration and buckling of super-elliptical plates under in-plane uniform pressure along the periphery, and results have been presented for different boundary conditions. The elaborated method of eigenfunction expansion in elliptic coordinates is employed by Hasheminejad et al. [6] to obtain an exact time-domain series solution involving products of angular and radial Mathieu functions for the forced flexural vibrations of a thin elastic plate of elliptical platform. Chai [7, 8] applied Rayleigh-Ritz method to study the buckling and post buckling of elliptical plate. In these studies, the large-deflection of elliptical plate is considered. Furthermore, a polynomial series expansion for displacements fields is used in conjunction with the Rayleigh-Ritz method to produce buckling and post buckling stress solutions for an elliptically-shaped surface layer. Bhushan et al. [9] used the finite element method to study the buckling and post buckling behavior of elliptical plates subject to uniform radial loading with different boundary conditions. Using the Rayleigh-Ritz method, Venkateswara et al. [10] studied the stability of simply supported and clamped elliptical plates subject to the compressive force uniformly distributed around the edge of the plate. The Rayleigh-Ritz method was used by Wang and Wang [11] to study the buckling and frequency of a super elliptic plate subject to uniform radial loading with clamped and simply

supported boundary conditions. The Rayleigh-Ritz method was used by Heitzer and Feucht [12] to study the buckling and post buckling of thin elliptical anisotropic plates with various boundary conditions. Using the Rayleigh-Ritz method, Mazhari and Shahidi [13] studied buckling and post buckling of circular plates with a non-concentric hole under uniform radial loading with various boundary conditions.

In this study, application of the Rayleigh-Ritz method by using in-plane and out-of-plane shape function and novel proper mapping is developed for studying the effect of the non-concentric elliptical hole on the critical buckling load factor of an elliptical plate that is subjected to the uniform in-plane loading along the periphery.

2. Coordinate System

In this paper, the natural coordinate system with the domain $[-1, 1]$ is used to simplify the integration process. The relationships between Cartesian and natural coordinate systems are expressed in the following equations and Figure 1:

$$r = (1 + \xi) + \frac{(1 - \xi)}{2},$$

$$\theta = \pi(1 + \eta),$$

$$u = \frac{r}{2}\cos\theta,$$

$$v = \frac{r}{2}\sin\theta,$$

$$x = u\left(a\left(2 - \frac{1}{\sqrt{u^2 + v^2}}\right) + 2c\left(\frac{1}{\sqrt{u^2 + v^2}} - 1\right)\right) + e(2\sqrt{u^2 + v^2} - 1),$$

$$y = v\left(b\left(2 - \frac{1}{\sqrt{u^2 + v^2}}\right) + 2d\left(\frac{1}{\sqrt{u^2 + v^2}} - 1\right)\right). \quad (1)$$

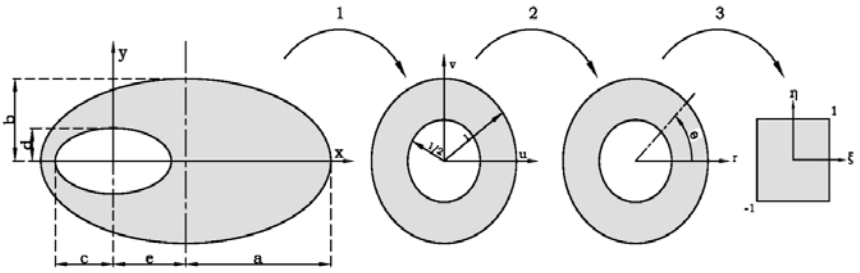

Figure 1. Schematic of changing of variable of an elliptical plate with non-concentric elliptical hole to natural coordinate system.

The differential operators of the two coordinate systems are related by

$$\begin{Bmatrix} \frac{\partial}{\partial \xi} \\ \frac{\partial}{\partial \eta} \end{Bmatrix} = \begin{pmatrix} \frac{\partial x}{\partial \xi} & \frac{\partial y}{\partial \xi} \\ \frac{\partial x}{\partial \eta} & \frac{\partial y}{\partial \eta} \end{pmatrix} \begin{Bmatrix} \frac{\partial}{\partial x} \\ \frac{\partial}{\partial y} \end{Bmatrix} = \mathbf{J} \begin{Bmatrix} \frac{\partial}{\partial x} \\ \frac{\partial}{\partial y} \end{Bmatrix}, \tag{2}$$

where **J** is the Jacobian matrix. Applying the chain rule of differentiation, and after some mathematical manipulation, it can be shown that the second derivatives can be expressed by

$$\begin{Bmatrix} \frac{\partial^2}{\partial x^2} \\ \frac{\partial^2}{\partial y^2} \\ \frac{\partial^2}{\partial x \partial y} \end{Bmatrix} = \mathbf{J}_2^{-1} \left(\begin{Bmatrix} \frac{\partial^2}{\partial \xi^2} \\ \frac{\partial^2}{\partial \eta^2} \\ \frac{\partial^2}{\partial \xi \partial \eta} \end{Bmatrix} + \mathbf{R} \begin{Bmatrix} \frac{\partial}{\partial \xi} \\ \frac{\partial}{\partial \eta} \end{Bmatrix} \right), \tag{3}$$

where

$$\mathbf{J}_2 = \begin{pmatrix} J_{11}^2 & J_{12}^2 & 2J_{12}J_{11} \\ J_{21}^2 & J_{22}^2 & 2J_{21}J_{22} \\ J_{11}J_{21} & J_{12}J_{22} & J_{11}J_{22} + J_{12}J_{21} \end{pmatrix} \tag{4}$$

and the transformation matrix **R** is defined as

$$\mathbf{R} = \begin{pmatrix} 0 & 0 \\ 0 & 0 \\ \alpha & \beta \end{pmatrix}, \tag{5}$$

where

$$\alpha = \frac{1}{|\mathbf{J}|}(J_{11,\eta}J_{22} - J_{22,\xi}J_{21}),$$

$$\beta = \frac{1}{|\mathbf{J}|}(J_{22,\xi}J_{11} - J_{11,\eta}J_{12}). \tag{6}$$

3. Interpolation of Displacement Fields and Shape Functions

Displacement field in mid-plane of the plate has three independent displacement components u, v and w corresponding to x, y and z as follows:

$$U_p = \langle u \quad v \quad w \rangle^T. \tag{7}$$

Using equation (1), the displacement fields in the natural coordinate system can be noted as:

$$u = \sum_{i=1}^{n} N_{ui}(\xi, \eta)\hat{u}_i,$$

$$v = \sum_{i=1}^{n} N_{vi}(\xi, \eta)\hat{v}_i,$$

$$w = \sum_{i=1}^{n} N_{wi}(\xi, \eta)\hat{w}_i, \tag{8}$$

where $\hat{w}_i$, $\hat{v}_i$, $\hat{u}_i$ are generalized coordinates and N_{ui} and N_{vi} are in-plane shape functions and N_{wi} is the out-of-plane shape function. Equation (8) is written in matrix form as

$$\begin{Bmatrix} u \\ v \\ w \end{Bmatrix} = \sum_{i=1}^{n} \begin{pmatrix} N_{ui} & 0 & 0 \\ 0 & N_{vi} & 0 \\ 0 & 0 & N_{wi} \end{pmatrix} \begin{Bmatrix} \hat{u}_i \\ \hat{v}_i \\ \hat{w}_i \end{Bmatrix} = U_p = \sum_{i=1}^{n} \mathbf{N}_i \mathbf{\Delta}_i, \tag{9}$$

where $\mathbf{\Delta}_i$ is the vector of degree of freedom or generalized coordinates and $\mathbf{N}_i$ is called the *matrix of shape functions*. The previous equation for general conditions can be expressed as:

$$U_p = \mathbf{N}\mathbf{\Delta}. \tag{10}$$

The shape functions are assumed as $\mathbf{N} = \sum_{i=1}^{n}\sum_{j=1}^{n} N_{y_i}(\eta)N_{x_j}(\xi)$, where $\mathbf{N}_y(\eta)$ is presented as:

$$\mathbf{N}_y(\eta) = \langle 1 \quad \sin(\pi(\eta+1)) \quad \cos(\pi(\eta+1)) \quad \sin 2(\pi(\eta+1)) \quad \cos 2(\pi(\eta+1)) \quad \cdots \rangle. \tag{11}$$

For the out-of-plane solution, the first four shape functions are Hermitian shape functions and the rest six shape functions are Hierarchical shape functions which are [16]

$$N_r(\xi) = \sum_{n=0}^{\frac{r}{2}} \frac{(-1)^n(2r-2n-7)!!}{2^n n!(r-2n-1)!}, \quad r > 4. \tag{12}$$

For the in-plane solution, the first two shape functions are Lagrangian shape functions and the rest eight shape functions are Hierarchical shape functions [16].

4. Buckling Analysis

The strain energy due to the bending moment in polar coordinate system is [1, 2]

$$U_b = \frac{1}{2}\int\int_A \boldsymbol{\kappa}^T \mathbf{D}_b \boldsymbol{\kappa} dA, \tag{13}$$

where $\mathbf{D}_b$ is the elasticity matrix of the plate, which can be written as

$$\mathbf{D}_b = D\begin{pmatrix} 1 & v & 0 \\ v & 1 & 0 \\ 0 & 0 & \frac{1-v}{2} \end{pmatrix}, \tag{14}$$

where $D = \dfrac{Et^3}{12(1-v^2)}$ is the flexural rigidity of the plate, v is the Poisson's ratio, t is the thickness of the plate, and E is the Young's modulus. The curvature vector in mid-plane of the plate is

$$\boldsymbol{\kappa} = \begin{Bmatrix} \kappa_x \\ \kappa_y \\ \kappa_{xy} \end{Bmatrix} = \begin{pmatrix} 0 & 0 & \dfrac{\partial^2}{\partial^2 x} \\ 0 & 0 & \dfrac{\partial^2}{\partial^2 y} \\ 0 & 0 & \dfrac{\partial^2}{\partial x \partial y} \end{pmatrix} \begin{Bmatrix} u \\ v \\ w \end{Bmatrix}. \tag{15}$$

Substituting equation (10) into (15), we have

$$\boldsymbol{\kappa} = \mathbf{L}_b U_p = \mathbf{L}_b \mathbf{N} \boldsymbol{\Delta} = \mathbf{B}_b \boldsymbol{\Delta}, \tag{16}$$

where $\mathbf{B}_b$ and $\mathbf{L}_b$ are matrices containing appropriate differential operators. Consequently, equation (13) can be rearranged as

$$U_b = \frac{1}{2} \int\int_A \boldsymbol{\Delta}^T \mathbf{B}_b^T \mathbf{D}_b \mathbf{B}_b \boldsymbol{\Delta} dA = \frac{1}{2} \boldsymbol{\Delta}^T \mathbf{K}_b \boldsymbol{\Delta}, \tag{17}$$

where $\mathbf{K}_b$ is the bending stiffness matrix of the plate and is

$$\mathbf{K}_b = \int\int_A \mathbf{B}_b^T \mathbf{D}_b \mathbf{B}_b dA. \tag{18}$$

The work done on the mid-plane of the plate due to the external forces is given by

$$W = \frac{1}{2} \int\int\int_\Omega \left\langle \frac{\partial w}{\partial x} \; \frac{\partial w}{\partial y} \right\rangle \begin{pmatrix} \sigma_x & \tau_{xy} \\ \tau_{xy} & \sigma_y \end{pmatrix} \begin{Bmatrix} \dfrac{\partial w}{\partial x} \\ \dfrac{\partial w}{\partial y} \end{Bmatrix} d\Omega, \tag{19}$$

where σ_x, σ_y and τ_{xy} are the in-plane stresses. By introducing the following matrix for buckling behavior of the plate:

$$\begin{pmatrix} 0 & 0 & \dfrac{\partial}{\partial x} \\ 0 & 0 & \dfrac{\partial}{\partial y} \end{pmatrix} \begin{Bmatrix} u \\ v \\ w \end{Bmatrix} = \mathbf{B}_G \boldsymbol{\Delta}, \tag{20}$$

equation (19) can be rewritten as

$$W = \frac{1}{2} \int\int\int_{\Omega} \boldsymbol{\Delta}^T \mathbf{B}_G^T \boldsymbol{\sigma} \mathbf{B}_G \boldsymbol{\Delta} d\Omega = \frac{1}{2} \boldsymbol{\Delta}^T \mathbf{K}_G \boldsymbol{\Delta}, \tag{21}$$

where $\mathbf{K}_G$ is the geometric stiffness matrix and is

$$\mathbf{K}_G = \int\int\int_{\Omega} \mathbf{B}_G^T \boldsymbol{\sigma} \mathbf{B}_G d\Omega, \tag{22}$$

where $\boldsymbol{\sigma}$ is the in-plane stress matrix. The total potential energy of the plate due to external forces exerted on mid-plane and bending is

$$\prod = U_b - W = \frac{1}{2} \boldsymbol{\Delta}^T \mathbf{K}_b \boldsymbol{\Delta} - \frac{1}{2} \boldsymbol{\Delta}^T \mathbf{K}_G \boldsymbol{\Delta}. \tag{23}$$

Based on the Rayleigh-Ritz method, the variation of the above equation should be equal to zero; therefore, we have

$$\delta \prod = \delta U_b + \delta W = \delta \boldsymbol{\Delta}^T (\mathbf{K}_b - \mathbf{K}_G) \boldsymbol{\Delta} = 0. \tag{24}$$

Since $\delta \boldsymbol{\Delta}^T$ non-zero

$$(\mathbf{K}_b - \lambda \mathbf{K}_G) \boldsymbol{\Delta} = 0. \tag{25}$$

The above equation is an eigen-value problem. The minimum eigen-value is the critical buckling load factor and its corresponding eigen-vector is the first buckling mode shape. The relation between the critical buckling load factor λ_{cr} and the critical applied traction load on the outer boundary N_{cr} is

$$N_{cr} = \lambda_{cr} \frac{D}{a^2}. \tag{26}$$

4.1. In-plane solution

The presence of a non-concentric elliptical hole along the horizontal axes

of an elliptical plate always causes non-symmetric distribution to the in-plane stresses when it is subjected to external in-plane radial loading. A problem such as this cannot be handled analytically; therefore, the numerical in-plane solution is the only way to find the in-plane stress distributions, which is presented as the following.

The strain energy due to in-plane deformation for small displacement is given as

$$U_{ml} = \frac{1}{2}\int\int_A \boldsymbol{\varepsilon}_{ml}^T \mathbf{D}_m \boldsymbol{\varepsilon}_{ml} dA, \tag{27}$$

where $\mathbf{D}_m$ is the stress-strain relationships matrix, and for the plane-stress problems, it is

$$\mathbf{D}_m = \frac{Et}{1-v^2}\begin{pmatrix} 1 & v & 0 \\ v & 1 & 0 \\ 0 & 0 & \dfrac{1-v}{2} \end{pmatrix}. \tag{28}$$

In-plane strains for small displacement are

$$\boldsymbol{\varepsilon}_{ml} = \begin{Bmatrix} \varepsilon_x \\ \varepsilon_y \\ \gamma_{xy} \end{Bmatrix} = \begin{Bmatrix} \dfrac{\partial u}{\partial x} \\ \dfrac{\partial v}{\partial y} \\ \dfrac{\partial u}{\partial y} + \dfrac{\partial v}{\partial x} \end{Bmatrix} = \begin{pmatrix} \dfrac{\partial}{\partial x} & 0 & 0 \\ 0 & \dfrac{\partial}{\partial y} & 0 \\ \dfrac{\partial}{\partial y} & \dfrac{\partial}{\partial x} & 0 \end{pmatrix} \begin{Bmatrix} u \\ v \\ w \end{Bmatrix} = \mathbf{L}_m U_p \tag{29}$$

or

$$\boldsymbol{\varepsilon}_{ml} = \mathbf{L}_m \mathbf{N} \boldsymbol{\Delta} = \mathbf{B}_m \boldsymbol{\Delta}, \tag{30}$$

where $\mathbf{L}_m$ and $\mathbf{B}_m$ are matrices containing appropriate differential operators. Consequently, equation (27) may be rewritten as

$$U_{ml} = \frac{1}{2}\int\int_A \boldsymbol{\Delta}^T \mathbf{B}_m^T \mathbf{D}_m \mathbf{B}_m \boldsymbol{\Delta} dA = \frac{1}{2}\boldsymbol{\Delta}^T \mathbf{K}_{ml} \boldsymbol{\Delta}, \tag{31}$$

where $\mathbf{K}_{ml}$ is the plate's membrane stiffness matrix and is given by

$$\mathbf{K}_{ml} = \int\int_A \mathbf{B}_m^T \mathbf{D}_m \mathbf{B}_m dA. \tag{32}$$

Using Figure 2, it is seen that the work done by the applied traction load $\mathbf{t}^T = \langle \sigma_n \ \tau \ 0 \rangle$ is

$$W_t = \int_\Gamma U_p \mathbf{t} \, d\Gamma = \int_\Gamma \mathbf{\Delta}^T \mathbf{N}^T \mathbf{t} \, d\Gamma = \mathbf{\Delta}^T \mathbf{F}, \tag{33}$$

where **F** is the generalized force vector given by

$$\mathbf{F} = \int_\Gamma \mathbf{N}^T \mathbf{t} \, d\Gamma. \tag{34}$$

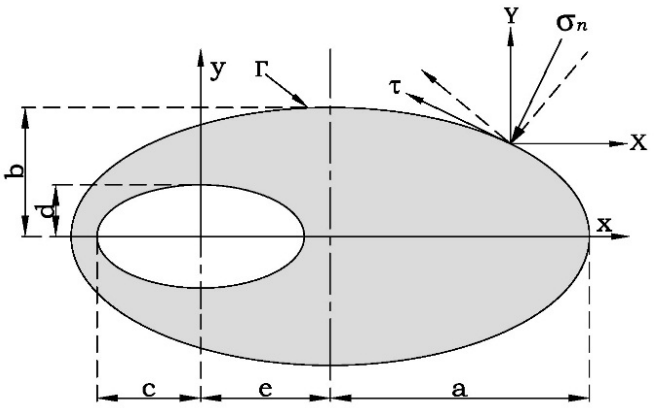

Figure 2. Schematic of applied in-plane load on the boundary of the elliptical plate.

Based on the Rayleigh-Ritz method, minimizing the total potential energy leads to static equilibrium, and we have

$$\delta \prod = \delta U_{ml} + \delta W_t = 0 = \delta \mathbf{\Delta}^T \mathbf{K}_{ml} \mathbf{\Delta} - \delta \mathbf{\Delta}^T \mathbf{F} = \mathbf{0} \tag{35}$$

which means

$$\mathbf{K}_{ml} \mathbf{\Delta} = \mathbf{F}. \tag{36}$$

On the other hand, the relation between stress and strain is

$$\boldsymbol{\sigma} = \begin{Bmatrix} \sigma_x \\ \sigma_y \\ \tau_{xy} \end{Bmatrix} = \frac{E}{1-v^2} \begin{pmatrix} 1 & v & 0 \\ v & 1 & 0 \\ 0 & 0 & \dfrac{1-v}{2} \end{pmatrix} \begin{Bmatrix} \varepsilon_x \\ \varepsilon_y \\ \gamma_{xy} \end{Bmatrix} = \mathbf{D}_s \boldsymbol{\varepsilon}_{ml}. \tag{37}$$

Substituting equation (30) into (37), we get

$$\boldsymbol{\sigma} = \mathbf{D}_s \mathbf{B}_m \boldsymbol{\Delta} \tag{38}$$

which after substituting from equation (36) becomes

$$\boldsymbol{\sigma} = \mathbf{D}_s \mathbf{B}_m \mathbf{K}_{ml}^{-1} \mathbf{F}. \tag{39}$$

In equation (39), the Lagrange multipliers method is used to constrain the membrane stiffness matrix (K_{ml}). By applying this constrain as the in-plane boundary condition, the membrane stiffness matrix would be invertible. According to the balance of in-plane forces subject to uniform compressive force distributed around the outer edge, reaction forces of these constrains are zero, and no stress concentration occurs.

5. Numerical Results

In this section, different case studies are simulated to study the critical buckling factor. MATLAB programming code has been developed to calculate the results. In this program, the number of out-of-plane and in-plane shape functions are considered to be eight in both directions and the Poisson's ratio is selected as 0.3. For all the case studies, the elliptical plate is subjected to in-plane uniform pressure along the periphery.

Figure 3 shows the critical buckling load factor versus different value of $\frac{b}{a}$ for simply supported and clamped boundary conditions. These values are compared with the results of [6, 9-11, 14] in Tables 1 and 2. This compression shows strong agreement between the presented results and references.

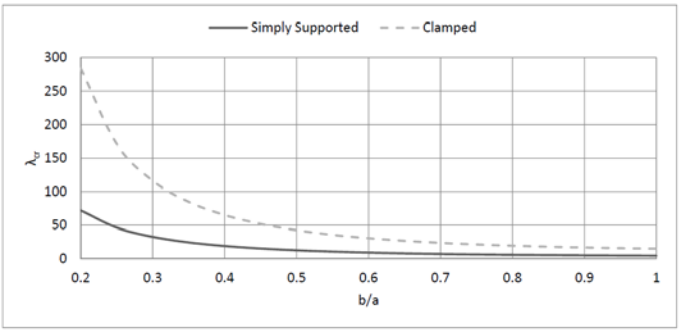

Figure 3. The value of the critical buckling load factor for clamped and simply supported boundary condition.

Table 1. Values of the critical buckling load factor λ_{cr} for an elliptical plate with a simply supported boundary condition

Methods	b/a								
	0.2	0.3	0.4	0.5	0.6	0.7	0.8	0.9	1
Ref. [6]	-	-	-	12.204	-	-	-	-	-
Ref. [9]	-	-	-	12.208	-	-	-	-	4.20
Ref. [10]	78.475	-	-	12.352	-	6.695	5.45	4.655	4.138
Ref. [11]	-	-	18.550	12.196	8.765	6.755	5.724	4.719	4.197
Present	72.034	32.476	18.706	12.257	8.785	6.754	5.515	4.723	4.204

Table 2. Values of the critical buckling load factor λ_{cr} for an elliptical plate with a clamped boundary condition

Methods	b/a								
	0.2	0.3	0.4	0.5	0.6	0.7	0.8	0.9	1
Ref. [6]	-	-	-	41.732	-	-	-	-	14.681
Ref. [9]	-	-	-	41.8492	-	-	-	-	14.695
Ref. [10]	272.25	-	-	43.32	-	23.656	19.304	16.629	14.68
Ref. [11]	-	-	63.305	41.738	30.180	23.429	19.182	16.493	14.681
Ref. [14]	281.25	-	-	40.2	-	23.997	19.507	16.81	14.8
Present	284.695	116.293	65.094	42.446	30.478	23.549	19.296	16.555	14.742

Tables 1 and 2 compare the effect of the ratio $\frac{b}{a}$ on the critical buckling load factor, where it was found that by increasing $\frac{b}{a}$ the critical buckling load factor was decreased. This decrease was very significant for the clamped boundary condition, especially where $\frac{b}{a}$ is between 0.2 and 0.5.

Figures 4 through 17 show the effect of the central elliptical hole on critical buckling load factor for clamped and simply supported boundary conditions.

Figure 18 shows a special case when $\frac{b}{a} = 1$ and $\frac{c}{a} = \frac{d}{b}$ (circular plate), which was studied previously by several researchers [13, 15]. Results of the special case are compared with the previous works and summarized in Tables 3 and 4. As it can be observed, the two results are in good agreement.

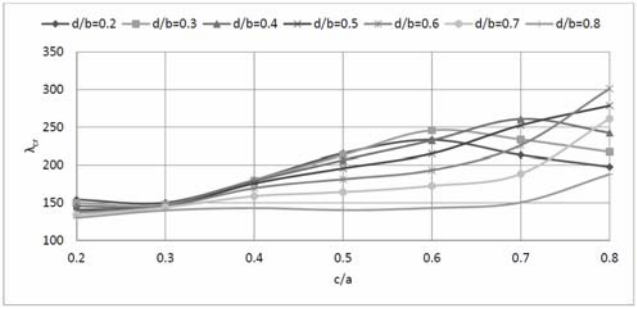

Figure 4. The value of the critical buckling load factor for elliptical plate with clamped boundary condition for $\frac{b}{a} = 0.2$.

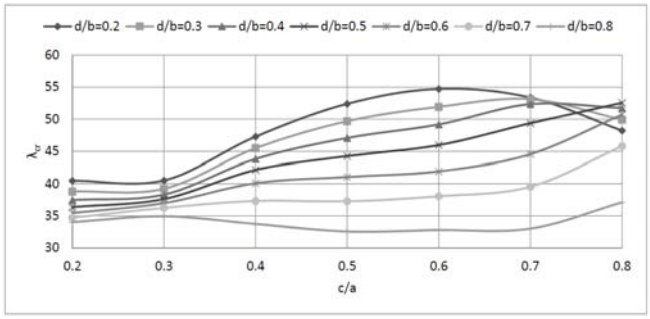

Figure 5. The value of the critical buckling load factor for elliptical plate with simply supported boundary condition for $\frac{b}{a} = 0.2$.

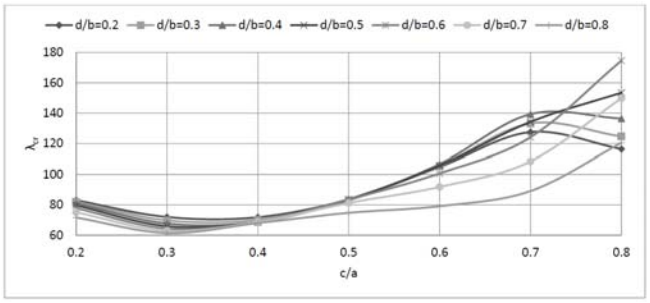

Figure 6. The value of the critical buckling load factor for elliptical plate with clamped boundary condition for $\frac{b}{a} = 0.3$.

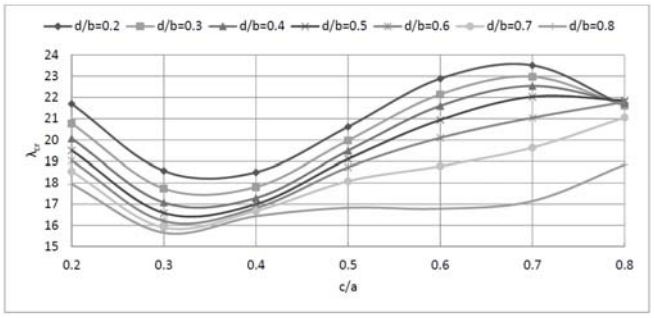

Figure 7. The value of the critical buckling load factor for elliptical plate with simply supported boundary condition for $\frac{b}{a} = 0.3$.

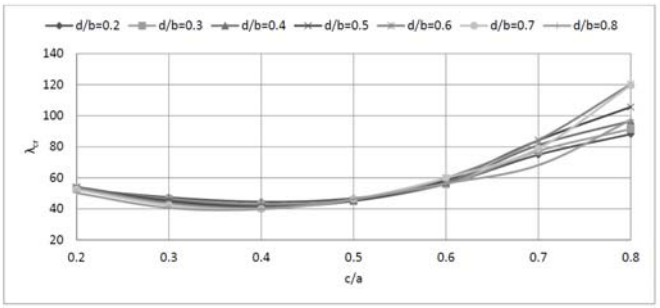

Figure 8. The value of the critical buckling load factor for elliptical plate with clamped boundary condition for $\frac{b}{a} = 0.4$.

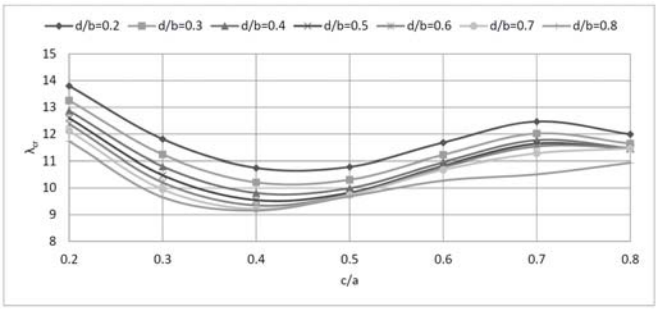

Figure 9. The value of the critical buckling load factor for elliptical plate with simply supported boundary condition for $\frac{b}{a} = 0.4$.

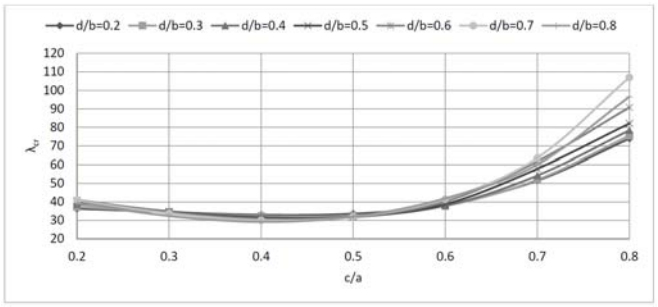

Figure 10. The value of the critical buckling load factor for elliptical plate with clamped boundary condition for $\frac{b}{a} = 0.5$.

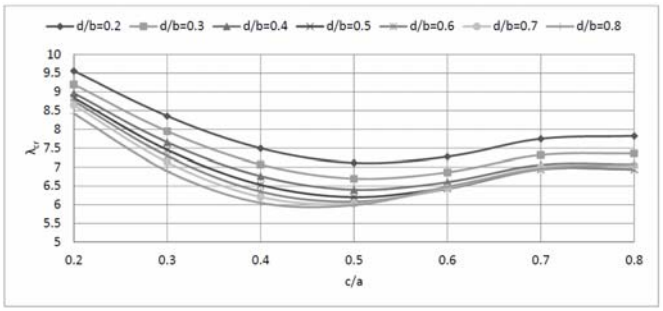

Figure 11. The value of the critical buckling load factor for elliptical plate with simply supported boundary condition for $\frac{b}{a} = 0.5$.

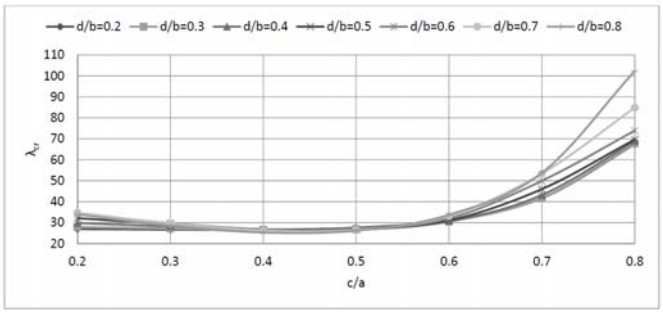

Figure 12. The value of the critical buckling load factor for elliptical plate with clamped boundary condition for $\frac{b}{a} = 0.6$.

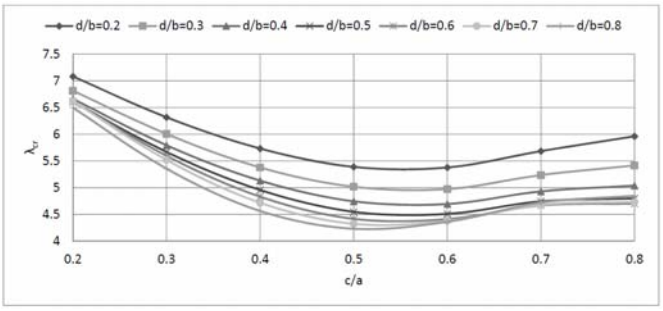

Figure 13. The value of the critical buckling load factor for elliptical plate with simply supported boundary condition for $\frac{b}{a} = 0.6$.

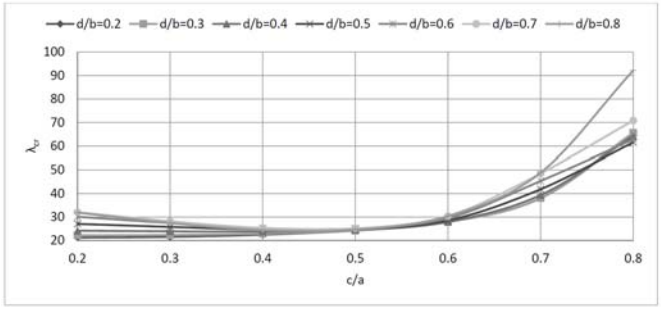

Figure 14. The value of the critical buckling load factor for elliptical plate with clamped boundary condition for $\frac{b}{a} = 0.7$.

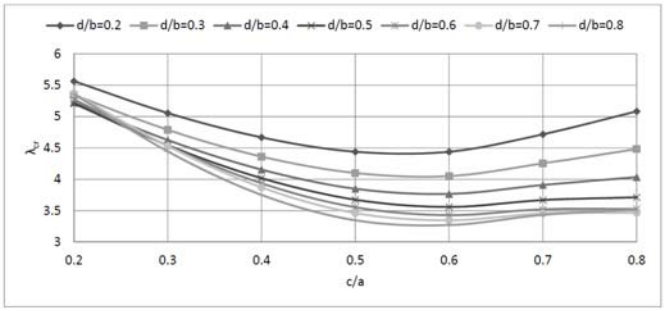

Figure 15. The value of the critical buckling load factor for elliptical plate with simply supported boundary condition for $\frac{b}{a} = 0.7$.

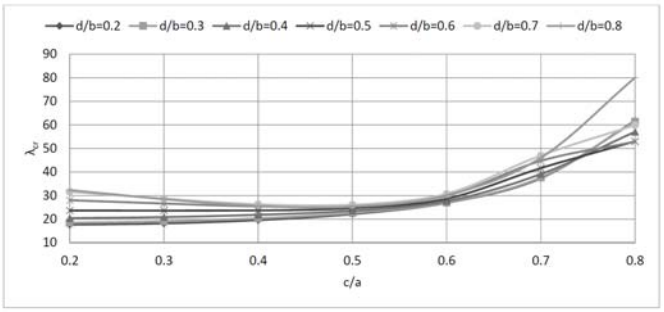

Figure 16. The value of the critical buckling load factor for elliptical plate with clamped boundary condition for $\frac{b}{a} = 0.8$.

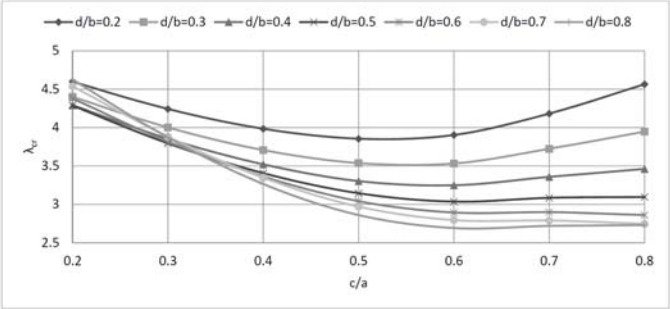

Figure 17. The value of the critical buckling load factor for elliptical plate with simply supported boundary condition for $\frac{b}{a} = 0.8$.

The general trend that can be observed from Figures 4 through 17, regardless of the boundary condition types, is that by increasing the ratio $\frac{b}{a}$, which means changing the geometry of the plate from elliptic to circular, the critical buckling load factor is reduced.

For the simply supported boundary condition cases, the critical buckling load factor is fluctuating, where it decreased for $0.2 \le \frac{c}{a} \le 0.5$, and increased after that. Moreover, the change in the critical buckling load factor magnitude is insignificant as the ratio of $\frac{b}{a}$ higher than 0.3. In addition, by increasing the ratio $\frac{d}{b}$, the critical buckling load factor is constantly decreasing. In contrast, with regards to the plates with clamped boundary conditions, the general trend for the critical buckling load factor is increasing for $\frac{b}{a} \ge 0.3$ as the ratio $\frac{c}{a}$ is higher than 0.4.

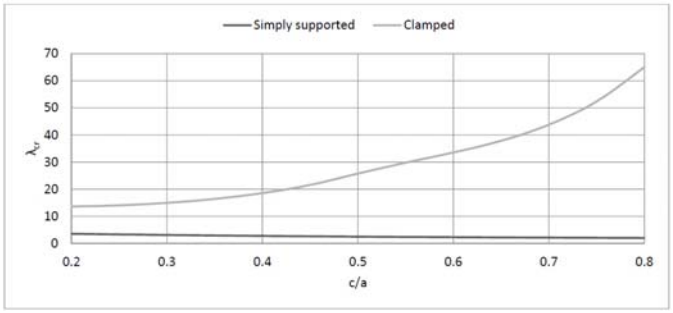

Figure 18. The value of the critical buckling load factor for circular plate with clamped and simply supported boundary condition.

Table 3. Values of the critical buckling load factor λ_{cr} for a circular plate with a clamped boundary condition

Methods	$c/a = d/b$					
	0.2	0.3	0.4	0.5	0.6	0.7
Ref. [13]	13.6039	14.9629	18.5557	25.7589	33.5123	43.69
Ref. [15]	13.32	14.52	17.64	24.84	-	-
Present	13.606	14.962	18.557	25.765	33.560	43.801

Table 4. Values of the critical buckling load factor λ_{cr} for a circular plate with a simply supported boundary

Methods	$c/a = d/b$					
	0.2	0.3	0.4	0.5	0.6	0.7
Ref. [13]	3.535	3.1054	2.763	2.5002	2.2973	2.138
Ref. [15]	3.60	3.24	2.76	2.52	-	-
Present	3.535	3.105	2.762	2.500	2.297	2.138

As shown in Figure 18 and Tables 3 and 4, in a circular plate with a simply supported boundary condition, increasing the $\frac{c}{a}$ value decreases the critical buckling load factor, and the first buckling mode shape looks like a domed curve. For the clamped boundary condition, the critical buckling load

factor decreases until $\frac{c}{a} \leq 0.55,$ then it increases. The reason for this is the changing of the first buckling mode shape [13].

Figures 19 through 32 show the effect of the non-concentric elliptical hole on the critical buckling load factor for clamped and simply supported boundary conditions. In a special case, when $\frac{b}{a} = 1$ and $\frac{c}{a} = \frac{d}{b}$ (circular plate), the effect of the non-concentric circular hole on the critical buckling load factor for clamped and simply supported boundary conditions are calculated and compared with the results of [13] in Tables 5 and 6. Also, the presented result is in good agreement with [13].

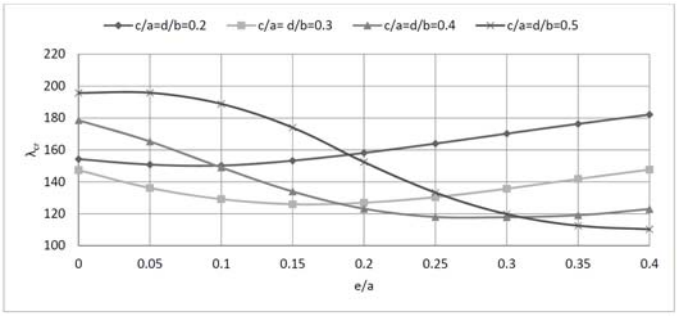

Figure 19. Effect of non-concentric on critical buckling load factor for elliptical plate with clamped boundary condition for $\frac{b}{a} = 0.2.$

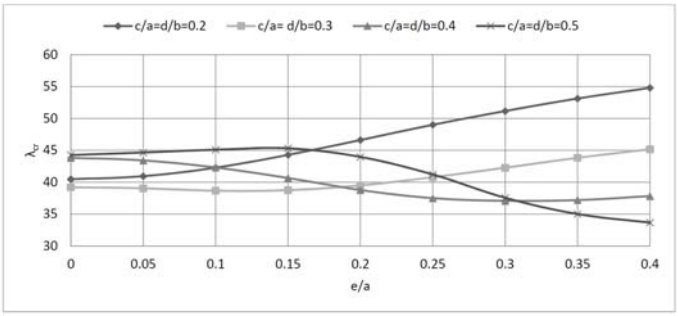

Figure 20. Effect of non-concentric on critical buckling load factor for elliptical plate with simply supported boundary condition for $\frac{b}{a} = 0.2.$

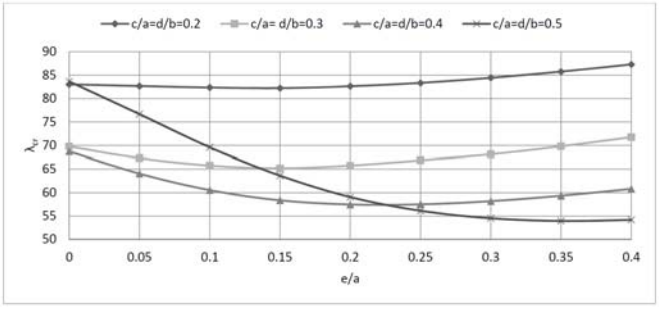

Figure 21. Effect of non-concentric on critical buckling load factor for elliptical plate with clamped boundary condition for $\frac{b}{a} = 0.3$.

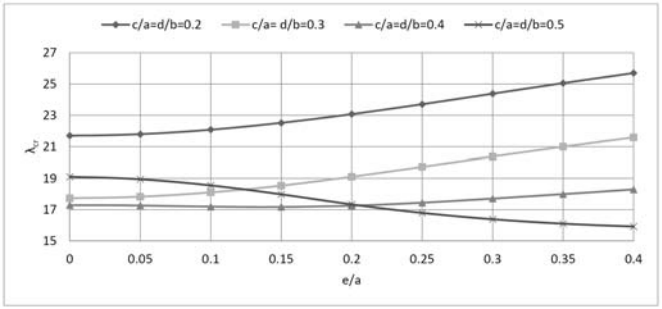

Figure 22. Effect of non-concentric on critical buckling load factor for elliptical plate with simply supported boundary condition for $\frac{b}{a} = 0.3$.

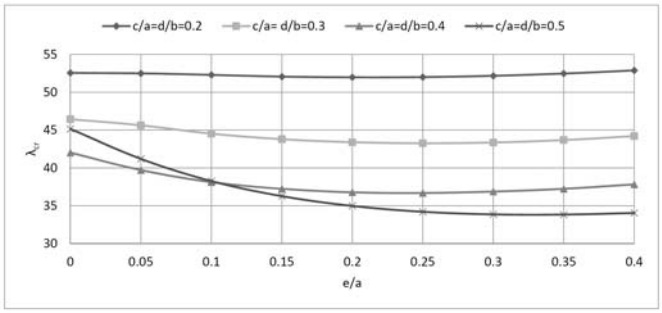

Figure 23. Effect of non-concentric on critical buckling load factor for elliptical plate with clamped boundary condition for $\frac{b}{a} = 0.4$.

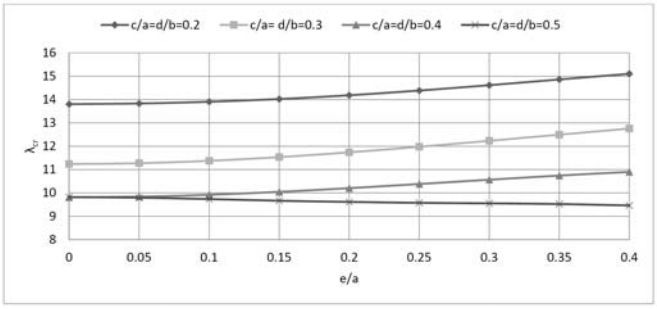

Figure 24. Effect of non-concentric on critical buckling load factor for elliptical plate with simply supported boundary condition for $\frac{b}{a} = 0.4$.

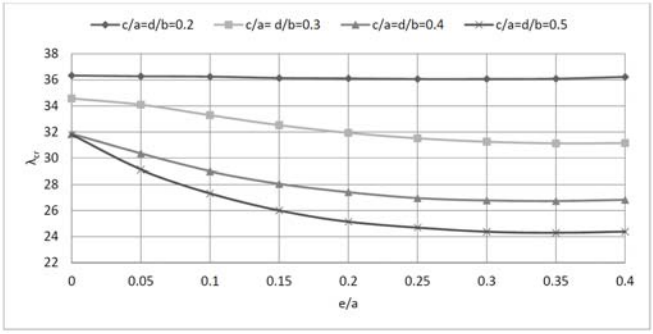

Figure 25. Effect of non-concentric on critical buckling load factor for elliptical plate with clamped boundary condition for $\frac{b}{a} = 0.5$.

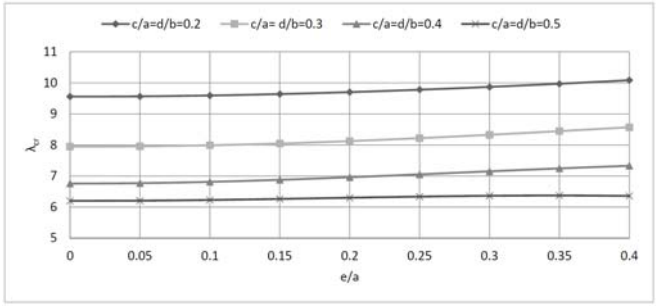

Figure 26. Effect of non-concentric on critical buckling load factor for elliptical plate with simply supported boundary condition for $\frac{b}{a} = 0.5$.

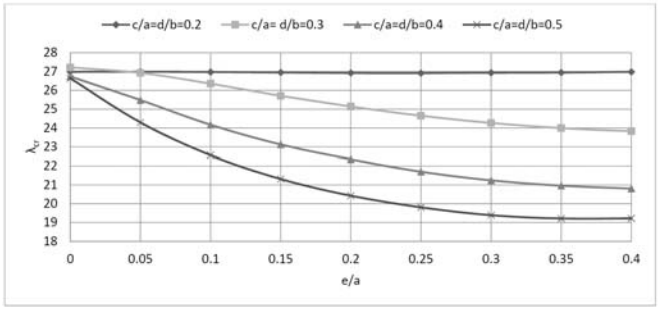

Figure 27. Effect of non-concentric on critical buckling load factor for elliptical plate with clamped boundary condition for $\frac{b}{a} = 0.6$.

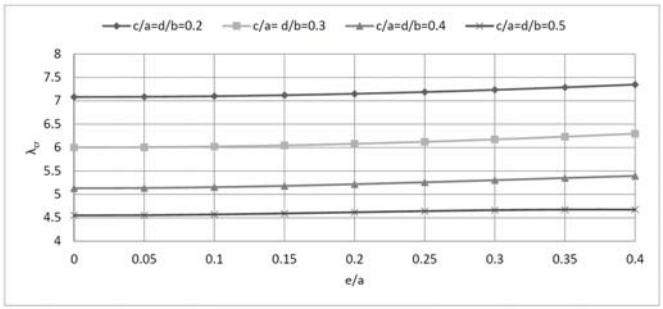

Figure 28. Effect of non-concentric on critical buckling load factor for elliptical plate with simply supported boundary condition for $\frac{b}{a} = 0.6$.

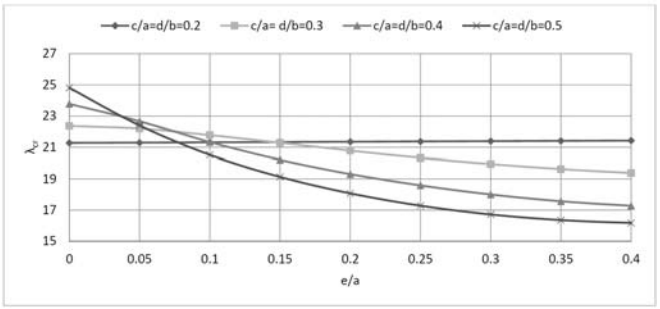

Figure 29. Effect of non-concentric on critical buckling load factor for elliptical plate with clamped boundary condition for $\frac{b}{a} = 0.7$.

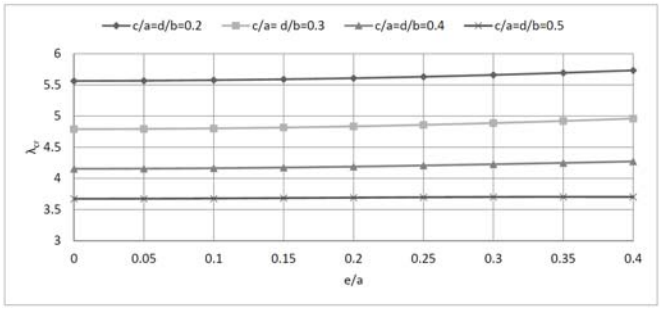

Figure 30. Effect of non-concentric on critical buckling load factor for elliptical plate with simply supported boundary condition for $\frac{b}{a} = 0.7$.

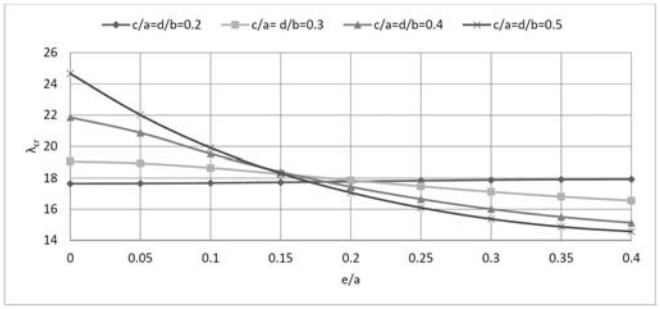

Figure 31. Effect of non-concentric on critical buckling load factor for elliptical plate with clamped boundary condition for $\frac{b}{a} = 0.8$.

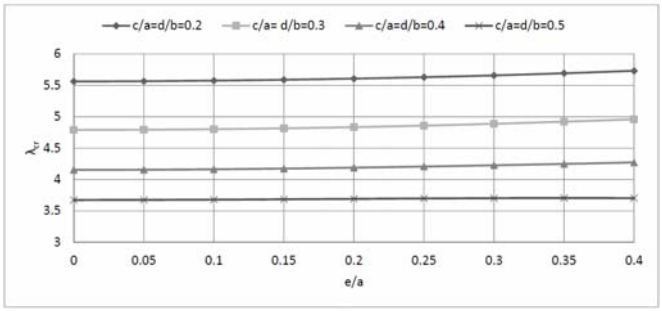

Figure 32. Effect of non-concentric on critical buckling load factor for elliptical plate with simply supported boundary condition for $\frac{b}{a} = 0.8$.

From the presented results, Figures 19 through 32, we can see that increasing the hole eccentricity for $\frac{b}{a} \geq 0.4$ has little effect on the critical buckling load factor for the simply support boundary cases. On the other hand, for the elliptical plates with the clamped boundary condition and $\frac{b}{a} \geq 0.4$, the critical buckling load factor is decreasing as the hole eccentricity is increased except when $\frac{c}{a} = 0.2$.

Table 5. Values of the critical buckling load factor λ_{cr} for a circular plate with non-concentric circular hole with a clamped boundary condition

b/a	e/a							
	0.1		0.2		0.3		0.4	
	Present	Ref. [13]	Present	Ref. [13]	Present	Ref. [13]	Present	Ref. [13]
0.2	13.66179	13.6489	13.80971	13.7923	13.97132	13.9546	14.06938	14.0453
0.3	14.76575	14.7611	14.31159	14.3014	13.79655	13.7645	13.33288	13.2141
0.4	17.018	17.0063	15.1467	15.1115	13.76248	13.6347	12.84662	12.4178
0.5	20.27445	20.2086	16.77126	16.5615	14.61959	14.0462	13.47544	11.9623

Table 6. Values of the critical buckling load factor λ_{cr} for a circular plate with non-concentric circular hole with a simply supported boundary condition

b/a	e/a							
	0.1		0.2		0.3		0.4	
	Present	Ref. [13]	Present	Ref. [13]	Present	Ref. [13]	Present	Ref. [13]
0.2	3.542399	3.5476	3.563933	3.5691	3.59767	3.6046	3.644834	3.6493
0.3	3.111889	3.1124	3.132943	3.1334	3.167379	3.1705	3.212167	3.2156
0.4	2.767117	2.7675	2.780587	2.781	2.802094	2.8016	2.833631	2.8241
0.5	2.500756	2.5008	2.50347	2.502	2.510404	2.4988	2.542105	2.4522

Tables 5 and 6 show the effect of non-dimensional distance of the non-concentric hole from the center of the circular plate on the critical buckling load factor for the simply supported and clamped boundary conditions, respectively. For elliptic plate with clamped boundary condition, increasing hole eccentricity resulted in decreasing the critical buckling factor. In contrast, plate with simply supported boundary condition increasing the hole eccentricity has insignificant effect on critical buckling factor.

6. Conclusion

The Rayleigh-Ritz method has been used as a numerical procedure to investigate the buckling analysis of elliptical plates with the non-concentric elliptical hole. The natural coordinate system has been employed to express the geometry of the plate in a simple form. By implementing the numerical procedure, 56 degrees of freedom are considered. This number of degrees of freedom plays an important role in the speed of solution.

In general, increasing the minor elliptic axis of the plate leads to decrease the critical buckling load factor. This decrease is more significant in cases where the clamped boundary condition is imposed.

The effect of the elliptic hole on the critical buckling load factor is fluctuating by decreasing first and then increasing as the major elliptic axis of the hole is increasing. The reason for this fluctuation is the change in the first buckling mode.

Lastly, the elliptic hole eccentricity has an insignificant effect on the critical buckling load factor in simply supported boundary conditions cases, whereas in the clamped boundary conditions, the critical buckling load factor is decreasing as the hole eccentricity is increased.

References

[1] S. Timoshenko and S. Woinowsky, Theory of Plate and Shells, McGraw-Hill, New York, 1972.

[2] A. C. Ugural, Stresses in Plates and Shell, McGraw-Hill, New York, 1981.

[3] S. R. Jazi and F. Farhatnia, Buckling analysis of functionally graded super elliptical plate using Pb-2 Ritz method, Advanced Materials Research 383-390 (2012), 5387-5391.

[4] B. S. Reddy and R. S. Alwar, Post-buckling analysis of orthotropic annular plates, Acta Mechanica 39 (1980), 289-296.

[5] Murat Altekin, Free linear vibration and buckling of super-elliptical plates resting on symmetrically distributed point-supports on the diagonals, Thin-Walled Structures 46 (2008), 1066-1086.

[6] Seyyed M. Hasheminejad, Shahed Rezaei and Rezgar Shakeri, Flexural transient response of elastically supported elliptical plates under in-plane loads using Mathieu functions, Thin-Walled Structures 62 (2013), 37-45.

[7] Herzl Chai, Buckling and post-buckling behavior of elliptical plates: Part I – Analysis, Journal of Applied Mechanics 57 (1990), 981-988.

[8] Herzl Chai, Buckling and post-buckling behavior of elliptical plates: Part II – Results, Journal of Applied Mechanics 57 (1990), 989-994.

[9] Bharat Bhushan, Gajbir Singh and G. Venkateswara Rao, Postbuckling of elliptical plates, Mechanics Research Communications 21 (1994), 89-94.

[10] A. Venkateswara Rao, B. Nageswara Rao and K. L. Prasad, Stability of simply supported and clamped elliptical plates, J. Sound Vibration 159(2) (1992), 378-381.

[11] C. M. Wang and L. Wang, Vibration and buckling of super elliptical plates, J. Sound Vibration 171 (1994), 301-314.

[12] J. Heitzer and M. Feucht, Buckling and postbuckling of thin elliptical anisotropic plates, Comput. & Structures 48 (1993), 983-992.

[13] E. Mazhari and A. L. Shahidi, Analysis of post buckling behavior of circular plates with non-concentric hole using the Rayleigh-Ritz method, Applied Mathematical Modelling 35 (2011), 3136-3153.

[14] Column Research Committee of Japan, Handbook of Structural Stability, Corona Publishing Company Ltd., Tokyo, 1971.

[15] Raymand J. Roark, Formulas for Stress and Strain, McGraw-Hill, New York, 1965.

[16] O. C. Zienkiewicz and R. L. Taylor, The Finite Element Method, Butterworth-Heinemann, 2000.